# Growth, structure, and magnetism of single-crystalline $Ni_xMn_{100-x}$ films and NiMn/Co bilayers on Cu(001)

C. Tieg, W. Kuch,* S. G. Wang,† and J. Kirschner
*Max-Planck-Institut für Mikrostrukturphysik, Weinberg 2, D-06120 Halle, Germany*
(Received 24 March 2006; revised manuscript received 8 June 2006; published 18 September 2006)

The growth and structure of single-crystalline $Ni_xMn_{100-x}$ films on Cu(001) were studied for concentrations of $x \geqslant 13$ and thicknesses of 0–15 monolayer (ML). Medium energy electron diffraction (MEED) curves revealed a layer-by-layer growth mode at a substrate temperature of $T=300$ K for alloy films with $40<x \leqslant 100$ and coverages up to 14 ML. A smooth transition to a three-dimensional growth is concluded from the decaying amplitude of the MEED oscillations as the Mn content increases. We find a characteristic $c(2\times2)$ superstructure by low-energy electron diffraction (LEED) for alloy compositions in the vicinity of the equiatomic region. A kinematic analysis of specular LEED intensity curves was employed to determine the average interlayer spacing $d$, yielding a decreasing $d$ with Ni content from 1.90 Å for $x=13$ to 1.73 Å for pure Ni on Cu(001). For equiatomic $c(2\times2)$ NiMn/Cu(001) we propose a bulklike $L1_0$ crystal structure, which is characterized by an in-plane orientation of the bulk $c$ axis. We show that Co grows layer by layer and assumes a $p(1\times1)$ structure on equiatomic $c(2\times2)$ NiMn/Cu(001). Using Co/Cu(001) as a substrate for equiatomic NiMn leads to a non-layer-by-layer growth of the alloy film and a diffuse LEED pattern with weak $c(2\times2)$ spots. The investigation of such bilayer structures by magneto-optical Kerr effect measurements (MOKE) indicates the presence of an antiferromagnetic (AFM) order in $Ni_xMn_{100-x}$ films with $x$ close to the equiatomic composition and thicknesses above 8 ML at 300 K, as concluded from the coercivity enhancement.

DOI: 10.1103/PhysRevB.74.094420 PACS number(s): 75.50.Ee, 68.55.−a, 75.70.−i

## I. INTRODUCTION

Much effort has been put in the past into the study of systems composed of an antiferromagnetic (AFM) and a ferromagnetic (FM) film. Such AFM/FM systems play an essential role in the field of magnetoelectronic devices, which rely on the exchange bias effect discovered half a century ago.[1] Despite the vast number of experimental and theoretical studies,[2,3] a general understanding of the magnetic interaction in AFM/FM systems is still missing. This is partly owing to the spin structure of the antiferromagnet with its spatial oscillation of the local spin direction with a period of the order of atomic distances. This greatly emphasizes the role of structural imperfections, the influence of even small degrees of nonuniformity, interface roughness, or the occurrence of chemical reactions at the interface in realistic AFM/FM systems, which are commonly composed of polycrystalline films. The situation is further complicated by the difficulty to probe the detailed spin structure in thin films, in particular, at interfaces.

Thus it is favorable to focus on well-defined model systems that allow us to manipulate the relevant physical parameters involved. Most frequently studied AFM/FM systems are based on the oxidic AFM systems NiO and CoO,[2,3] which possess experimentally convenient Néel temperatures. The Mn-based AFM system FeMn obtained similar importance, not only due to its technological relevance for exchange-biased magnetic tunnel junctions,[4] but also because single-crystalline FeMn can be stabilized as smooth and well-ordered films with a bulklike atomic and spin structure on Cu(001).[5,6] Another member of the Mn-based AFM metals is the $L1_0$ phase of NiMn. This system has attracted considerable attention as a pinning layer in spin-valve systems[7–9] because it provides a high blocking temperature and large exchange bias fields at the operation temperature of such magnetoresistive devices. However, the polycrystalline NiMn films in these multilayered structures demand a postdepositional annealing step[10–12] in order to induce a structural phase transition from the disordered fcc to the $L1_0$ phase, which is accompanied by a magnetic phase transition from paramagnetic to antiferromagnetic.

Our investigation of single-crystalline NiMn films is motivated by the prospect of studying the influence of a different AFM spin structure in the film and at the interface on the magnetic interaction in AFM/FM systems in comparison to model systems based on FeMn. In contrast to the noncollinear $3Q$ spin structure of chemically disordered fcc bulk FeMn, bulk NiMn exhibits a collinear AFM spin structure in the low temperature $L1_0$ phase for Ni contents $x$ in the range from ~45 to ~55.[13,14] The AF I-type spin structure of $L1_0$ NiMn is characterized by an antiparallel alignment of the magnetic moments of nearest-neighbor Mn atoms. The moments are oriented normal to the $c$ axis of the fct lattice.[15–18] The Néel temperature $T_N$ is as high as 1070 K,[19] and the lattice constants are equal to 3.74 and 3.52 Å along the $a$ and $c$ axis, respectively.[14,19] Single crystalline NiMn films have previously been prepared with thicknesses of up to 8 monolayer (ML) by the deposition of up to 4 ML Mn on Ni(001) at a substrate temperature of 600 K followed by an annealing step at the same temperature.[20,21] These surface alloys exhibit a characteristic $c(2\times2)$ superstructure due to the chemical order in conjunction with a large outward relaxation of the Mn atoms in the topmost layer. An x-ray magnetic circular dichroism study of $c(2\times2)$ NiMn/Ni(001) revealed an FM instead of an AFM order in the alloy, which was attributed to the lattice distortion.[22] FM order has also been shown for Ni-rich single-crystalline $Ni_xMn_{100-x}$ films with $x \geqslant 83$ on Cu(001).[23] These films were found to exhibit

 

a Ni-type spin-reorientation transition from in-plane to out-of-plane upon increasing the film thickness.

The aim of this work is to determine the growth, structure, and magnetic properties of $Ni_xMn_{100-x}$ films with a focus on equiatomic alloy films in the monolayer thickness regime. The study includes bilayers of $Ni_xMn_{100-x}$ and Co. The choice of Cu(001) as a substrate excludes the possibility of an induced FM order in NiMn and promotes an epitaxial relationship due to the small lattice mismatch with bulk $L1_0$ NiMn. We show that $Ni_xMn_{100-x}$ grows layer by layer on Cu(001) at 300 K for $x>40$, as concluded from the presence of oscillations of the medium energy electron-diffraction intensity. We observe that $Ni_xMn_{100-x}$/Cu(001) samples with $x$ in the vicinity of equiatomic concentration exhibit a characteristic $c(2\times2)$ superstructure, which is attributed to a bulk-like film structure. Our magnetic characterization of Co/NiMn bilayers by means of magneto-optical Kerr effect measurements indicates that an AFM order is indeed established in the equiatomic alloy at 300 K for film thicknesses above 8 ML.

## II. EXPERIMENTAL ASPECTS

Sample preparation and characterization were performed under ultrahigh vacuum conditions. The chemical cleanliness of the single-crystalline Cu(001) substrate was verified by Auger electron spectroscopy (AES) after repetitive cycles of sputtering with Argon (1 keV) at 300 K and annealing at 800 K. The films were grown on the clean substrate held at 300 K by electron-beam-assisted thermal evaporation of high purity material (Co, Ni: 99.99%, Mn: 99.95%) from three separate sources. A pressure in the $10^{-10}$ mbar range could be maintained during the operation of the evaporators. The $Ni_xMn_{100-x}$ films were prepared by the simultaneous evaporation of Ni and Mn. The alloy film composition $x$ was varied by adjusting the individual deposition rates. Medium energy electron diffraction (MEED) with a primary electron-beam energy of 3–4 keV was employed to monitor the epitaxial growth. The sample was aligned to grazing incidence of the electron beam with the [100] in-plane direction oriented parallel to the plane of incidence. The specular MEED intensity was recorded on a fluorescent screen opposite of the electron gun. The growth rate, ranging from 0.1 to 1 ML per min, was obtained from the period of the MEED oscillations. The composition $x$ was determined from the $Ni_xMn_{100-x}$ growth rate $r_{NiMn}$ and the Ni growth rate $r_{Ni}$ according to $x=r_{Ni}/r_{NiMn}$, while $r_{Ni}$ was calibrated by a separate deposition of Ni on Cu(001) at 300 K. Both growth rates could be obtained from MEED oscillations with an accuracy better than 5%, leading to an uncertainty in the composition $\Delta x/x$ of about 0.1. In addition, AES was used to check the reproducibility by the comparison of the ratios of Ni versus Mn AES peak intensity from separate film preparations.

The film structure was probed by low-energy electron diffraction (LEED). The film's lattice spacing along the surface normal was obtained from a kinematic analysis of LEED intensity versus energy [LEED $I(E)$] curves of the (0 0) LEED spot as described elsewhere.[5] The LEED $I(E)$ curves were measured at an inclination angle of 5° with respect to the sample normal. The magnetic properties of NiMn/Co bilayers were studied by magneto-optical Kerr effect measurements using a similar setup as described in Ref. 24. Our modified version employs an intensity-stabilized 5 mW laser diode emitting at a wavelength of 670 nm. The maximum accessible magnetic field at the sample is about 15 kA/m. A field-cooling procedure was not applied to our samples.

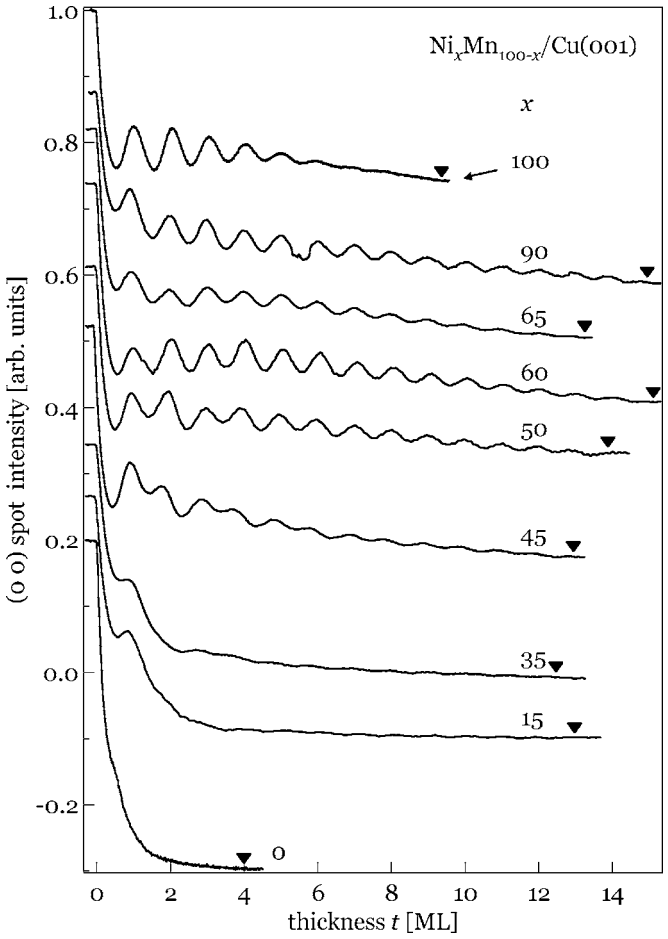


FIG. 1. MEED curves of the (0 0) spot recorded during the deposition of $Ni_xMn_{100-x}$ films on Cu(001) at $T=300$ K for various values of $x$. The closing of the shutters is indicated by a triangle at each curve. An oscillating MEED intensity is a fingerprint of a layer-by-layer growth mode. The MEED curves were normalized at $t=0$ ML to one and shifted vertically with respect to the curve of Ni/Cu(001) for clarity.

## III. RESULTS

### A. Growth and structure

The growth of $Ni_xMn_{100-x}$ on Cu(001) at $T=300$ K was investigated by means of MEED for the whole concentration range from pure Ni to pure Mn. Figure 1 shows the specular MEED intensity as a function of deposition time for increasing Ni content $x$ from bottom to top. The curves were normalized to the initial MEED intensity at the time before opening the shutters, i.e., at $t=0$ ML, and shifted vertically for clarity. The deposition time was converted into a mono-

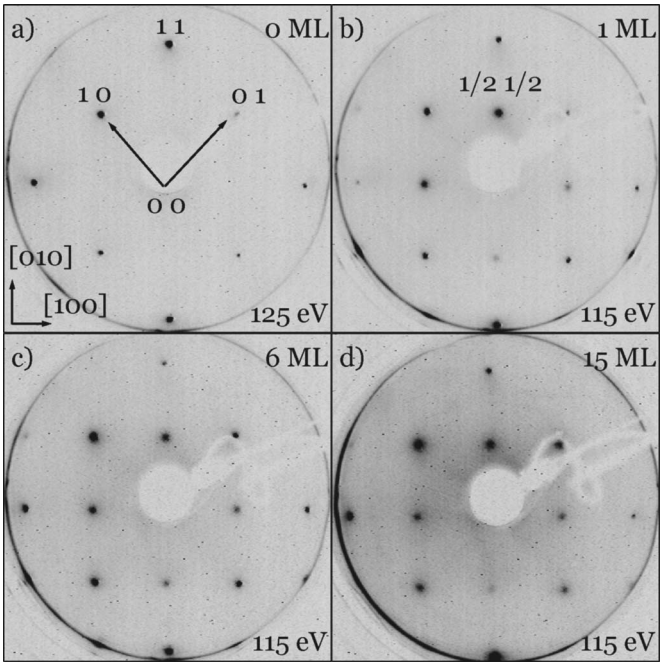


FIG. 2. LEED patterns of clean Cu(001) (a) and equiatomic NiMn films on Cu(001) for film thicknesses of 1 ML (b), 6 ML (c), and 15 ML (d). Note the strong $c(2\times2)$ superstructure spots at (1/2 1/2) positions in panels (b)–(d). Bulk crystallographic directions are indicated at the bottom left of (a). The electron energy is given at the bottom right of each pattern.

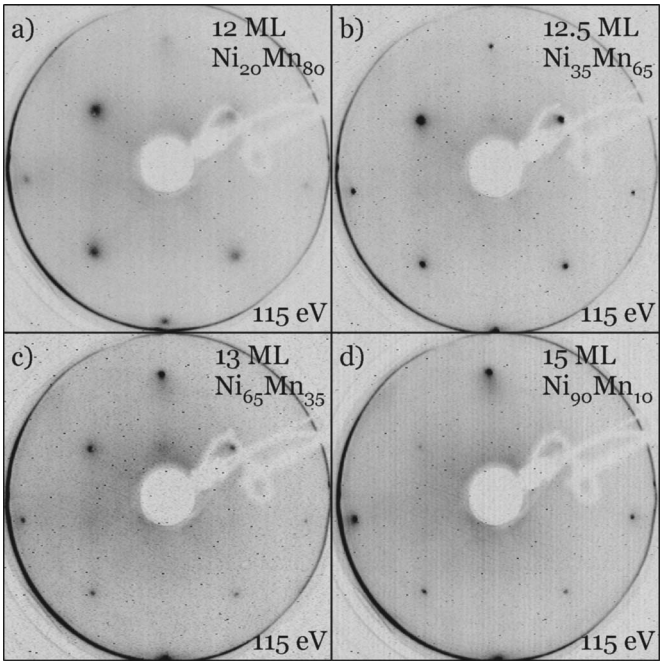


FIG. 3. LEED patterns of nonequiatomic $Ni_xMn_{100-x}$ films grown on Cu(001) at $T=300$ K: (a) 12 ML $Ni_{20}Mn_{80}$, (b) 12.5 ML $Ni_{35}Mn_{65}$, (c) 13 ML $Ni_{65}Mn_{35}$, and (d) 15 ML $Ni_{90}Mn_{10}$.

layer thickness scale under the assumption that a maximum in the MEED intensity corresponds to a filled integer monolayer, neglecting a possible phase shift. This conversion allows a convenient presentation of MEED curves obtained from films deposited at different growth rates in a single diagram. An oscillating MEED intensity, which is a fingerprint of a layer-by-layer growth mode, was found for $Ni_xMn_{100-x}$ films with a Ni content above 40%. The MEED oscillations for $40\leqslant x\leqslant 90$ extend to coverages above 10 ML, indicating an improved layer-by-layer growth in comparison to Ni/Cu(001), which exhibits only five pronounced maxima. Decreasing the Ni content below 40% gives rise to a smooth change from a layer-by-layer to a three-dimensional growth mode. The Mn-rich films in Fig. 1 ($x=35$ and 15) show a strongly decaying MEED intensity after developing a weak maximum at 1 ML coverage. The growth of Mn on Cu(001) is characterized by an even stronger decay of the MEED intensity and the absence of any oscillations.

Our study also included growth experiments of nearly equiatomic $Ni_xMn_{100-x}$ films on the same substrate at low temperatures. The MEED curve (not shown) obtained from 13 ML $Ni_{55}Mn_{45}$ grown at 190 K is characterized by a strongly decaying intensity at the initial growth (<2 ML) and a constant value at higher coverages in contrast to an oscillating intensity at 300 K.

The structure of $Ni_xMn_{100-x}$ on Cu(001) was found to depend on the composition. Figure 2 shows the LEED patterns with the first-order spots of the clean Cu(001) substrate [Fig. 2(a)] in comparison to equiatomic NiMn deposited on Cu(001) at 300 K for film thicknesses of 1, 6, and 15 ML [Figs. 2(b)–2(d)]. The $p(1\times1)$ unit cell of Cu(001) is indicated by the arrows in Fig. 2(a). Additional spots at (1/2 1/2) positions appear in the case of equiatomic NiMn films [Figs. 2(b)–2(d)]. Similar $c(2\times2)$ LEED patterns were observed for thicknesses up to 20 ML. The $c(2\times2)$ superstructure spots were found to have their maximal intensity at an electron energy of about 115 eV.

Nonequiatomic NiMn films on Cu(001) are characterized by $p(1\times1)$ LEED patterns. Figure 3 shows in the upper panel the patterns of the Mn-rich films of [Fig. 3(a)] 12 ML $Ni_{20}Mn_{80}$ and [Fig. 3(b)] 12.5 ML $Ni_{35}Mn_{65}$. The lower panel contains the patterns of the Ni-rich films of [Fig. 3(c)] 13 ML $Ni_{65}Mn_{35}$ and [Fig. 3(d)] 15 ML $Ni_{90}Mn_{10}$. These patterns were recorded at the same energy of 115 eV where the strong $c(2\times2)$ superstructure spots of the equiatomic NiMn films appeared. No superstructure spots were observed upon varying the energy. We found that $c(2\times2)$ superstructure spots are characteristic for $Ni_xMn_{100-x}$ films in the vicinity of equiatomic composition, e.g., $40\leqslant x\leqslant 60$. The superstructure spots are absent for Ni- and Mn-rich films [except for low coverages (<1 ML) of Mn on Cu(001) (Ref. 25)] and appear upon approaching the equiatomic composition, as can be deduced from Fig. 3(c), which already exhibits a faint intensity at half-order positions.

In order to address the crystallographic structure of $Ni_xMn_{100-x}$/Cu(001) along the surface normal, LEED $I(E)$ curves of the (0 0) spot were recorded and analyzed by a kinematic approach, yielding the average interlayer spacing $d$ of the top atomic layers. Figure 4(a) depicts the LEED $I(E)$ curves of clean Cu(001) and of a series of $Ni_xMn_{100-x}$ films for increasing Ni content from top to bottom. Alloy composition $x$ and thickness $t$ are indicated at the right. Each LEED $I(E)$ curve exhibits three maxima above 250 eV, which could

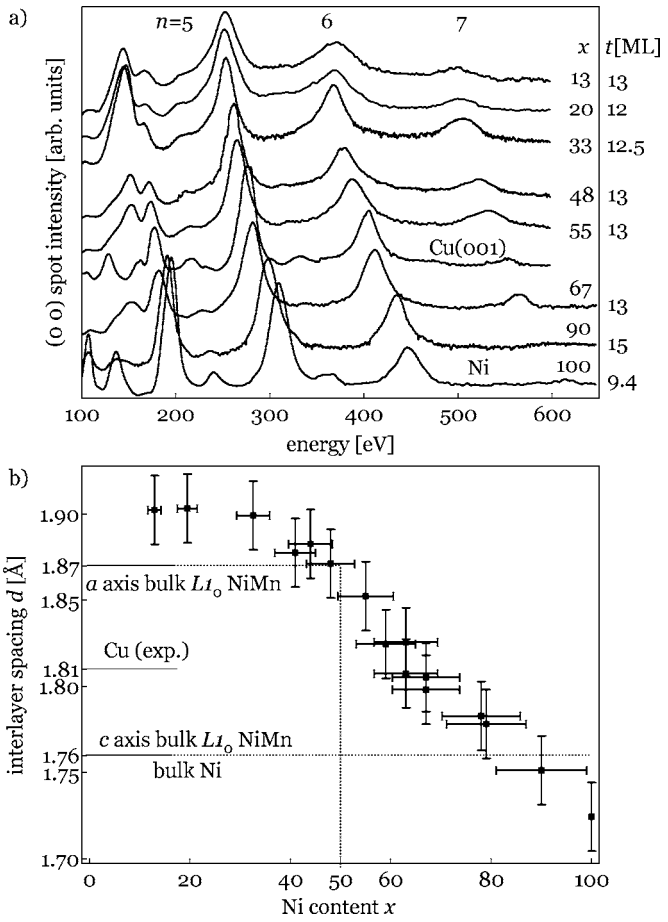


FIG. 4. LEED $I(E)$ study of $Ni_xMn_{100-x}$ films on Cu(001). (a) Intensity vs energy curves of the (0 0) LEED spot. The Ni content $x$ and film thickness $t$ are indicated at the right of each curve. The order of diffraction $n$ of the primary maxima is given at the top. Note the shift of the peaks to higher energies with increasing $x$. The curves were normalized to the peak height of the fifth-order maximum and shifted vertically for clarity. (b) Interlayer spacing $d$ vs $x$. Note that $d$ of equiatomic NiMn films coincides with the value along the bulk $a$ axis of $L1_0$ NiMn.

be identified as the fifth-, sixth-, and seventh-order Bragg maximum. Maxima of higher order were not found due to the decreasing peak intensity with increasing order. The identification of lower-order maxima ($n<5$) was hindered by the presence of strong multiple-scattering peaks. One notices a monotonic shift of the peak positions as a function of composition. For example, the fifth-order peak moves from ~250 to ~310 eV throughout the concentration series upon increasing $x$.

In the kinematic approach for the analysis of LEED $I(E)$ data, the average interlayer spacing $d$ is determined by the energetic positions $E_n$ of the Bragg maxima. Here, $d$ is obtained from a linear regression of an $E_n$ versus $n^2$ plot by applying the relation[5] $E_n=h^2n^2/(8m_e\cos^2\alpha\, d^2)+V_0$, where $h$, $m_e$, and $\alpha$ denote Planck's constant, electron mass, and incidence angle relative to the sample normal, respectively. The real part of the inner potential $V_0$ ($V_0<0$) takes into account the energy gain of the electrons upon entering the solid from the vacuum. $V_0$ was fixed to −10 eV, and was found to have no significant effect on the fit results within the reasonable range of −15 to −5 eV. For $E_n$, we simply used the energies of maximum peak intensity. The uncertainty (<10 eV) was found to have a negligible effect on $d$.

The average interlayer spacing $d$ of $Ni_xMn_{100-x}$ films on Cu(001) is shown as a function of $x$ in Fig. 4(b). The film thickness $t$ ranges from 11.5 to 15 ML, except for the pure Ni film, which has a thickness of 9.4 ML only. Most films had a thickness of 12–13 ML. The choice of film thickness above 9 ML was made in order exclude a contribution from the substrate to the LEED $I(E)$ curves. As an example, a film thickness of 9.4 ML Ni on Cu(001) corresponds to a thickness of 16 Å. This length scale is larger than the electron's inelastic mean free path[26] in Ni at 600 eV of 10.4 Å. Similar LEED $I(E)$ information depths are expected for the alloy films since the electron's inelastic mean free path does not strongly vary between neighboring $3d$ transition metals. The dotted horizontal lines at 1.87 and 1.76 Å indicate the interlayer spacings in bulk $L1_0$ NiMn along the $a$ and $c$ axis, respectively. The latter distance coincides with the value of bulk fcc Ni. The experimental value of 1.81 Å of Cu(001) is indicated by a solid line, and agrees with the value of bulk fcc Cu (1.808 Å). The average interlayer spacing of the alloy films decreases from 1.90 Å at $x=13$ to 1.73 Å at $x=100$. The known tetragonal lattice distortion of a Ni film on Cu(001),[27] which is characterized by an expansion of the fcc Ni lattice within the surface plane and a compression along the surface normal, could be reproduced, as can be concluded by the lower average interlayer spacing in comparison to the Ni bulk value. This illustrates the reliability of the kinematic approach. The most important result of the LEED $I(E)$ experiments is the fact that equiatomic $c(2\times2)$ NiMn films on Cu(001) exhibit a lattice spacing which matches the value along the $a$ axis of bulk NiMn.

We will now turn to bilayer systems composed of equiatomic NiMn and Co. NiMn/Co bilayers were prepared by subsequent depositions at 300 K without an intermediate annealing step. It was found that the growth of NiMn on Co/Cu(001) differs from the growth on Cu(001). Figure 5 compares the MEED curve of Co/NiMn/Cu(001) with the one of NiMn/Co/Cu(001). In Fig. 5(a) the deposition of 12 ML equiatomic NiMn on Cu(001) was followed by a deposition of 4 ML Co. The hatched area indicates a short delay of a few minutes between both depositions. The initial MEED intensity of the subsequent deposition was normalized to the MEED intensity present at the end of the first deposition. As can be concluded from the oscillating MEED intensity, a layer-by-layer growth is present throughout the whole bilayer deposition. In addition, the oscillating MEED intensity during the deposition of Co is superimposed on a background, which increases in intensity with coverage. One notices that the final MEED intensity at the fourth Co ML does even exceed the intensity at the beginning of the Co deposition. This suggests a decreasing surface roughness at integer monolayer coverage, i.e., a lower number of open surfaces, or a smaller fraction of the area occupied by noncompleted monolayers. The MEED curve recorded during the deposition with a reversed layer sequence is depicted in Fig. 5(b). The prominent MEED oscillations from the well-

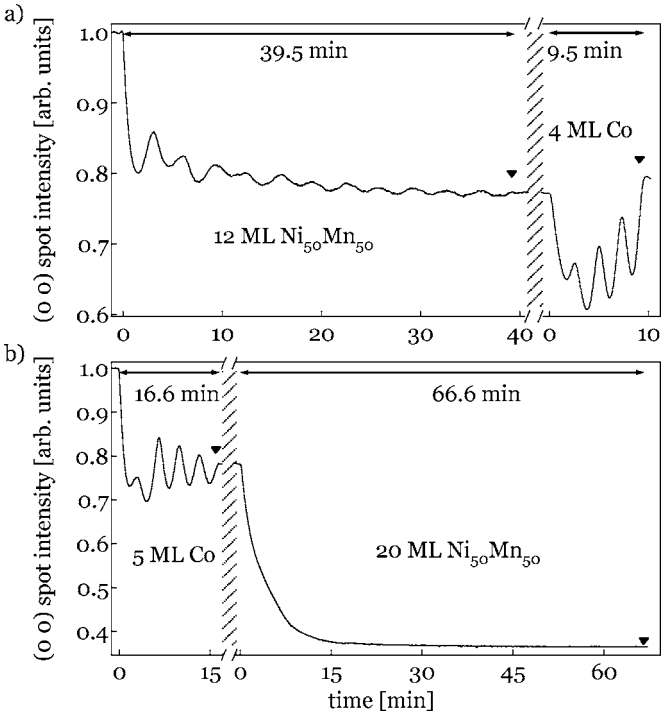


FIG. 5. MEED curves of the (0 0) spot recorded during the growth of NiMn/Co bilayers on Cu(001) at $T$=300 K: 4 ML Co/12 ML $Ni_{50}Mn_{50}$/Cu(001) (a), 20 ML $Ni_{50}Mn_{50}$/5 ML Co/Cu(001) (b). The shutter was opened at 0 min and closed at the time indicated by a triangle. Deposition times are given at the top of each curve.

known nearly perfect two-dimensional growth of Co on Cu(001) (Ref. 28) are followed by a featureless decaying MEED intensity during the subsequent growth of NiMn. The low MEED intensity, which levels off at 50% of the initial value (at $t_{NiMn}$=0 ML), and the absence of oscillations indicates a three-dimensional (3D) growth of equiatomic NiMn on 5 ML Co/Cu(001).

The LEED patterns of NiMn/Co bilayers are shown in Fig. 6. The left panel depicts the $p(1\times1)$ pattern of 6 ML Co/13 ML $Ni_{55}Mn_{45}$/Cu(001). Prior to the deposition of the Co film, the nearly equiatomic 13 ML $Ni_{55}Mn_{45}$ film exhibited a $c(2\times2)$ pattern at 115 eV similar to the patterns in Fig. 2. Although the pattern of the bilayer was recorded at

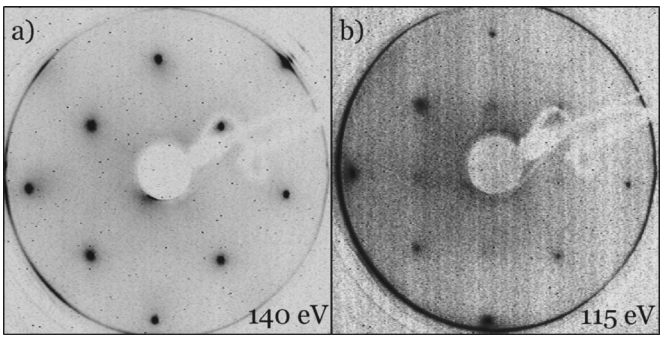


FIG. 6. LEED patterns of (a) 6 ML Co/13 ML $Ni_{55}Mn_{45}$/Cu(001) and (b) 8 ML $Ni_{50}Mn_{50}$/5 ML Co/Cu(001). Note the faint $c(2\times2)$ superstructure spots in (b).

140 eV instead of 115 eV, no superstructure spots were found upon varying the energy. The presence of a sharp $p(1\times1)$ LEED pattern verifies not only good epitaxial growth of Co on NiMn/Cu(001), but also a Co film structure, which is similar to the structure of fct Co/Cu(001).[29] Figure 6(b) depicts the LEED pattern of 8 ML $Ni_{50}Mn_{50}$ on top of 5 ML Co/Cu(001). Though the spots are low in intensity, a weak $c(2\times2)$ superstructure pattern can still be recognized. The weak diffraction pattern in comparison to the patterns of $c(2\times2)$ NiMn/Cu(001) in Fig. 2 is a result of the 3D growth mode of NiMn on Co/Cu(001), which gives rise to a rough surface [cf. Fig. 5(b)].

### B. Magnetic properties

In agreement with the bulk-phase diagram, which exhibits an AFM phase for $L1_0$ NiMn with a Néel temperature of 1070 K,[19] no FM signal was measured by means of MOKE in longitudinal and polar geometry for $Ni_xMn_{100-x}$/Cu(001) within the vicinity of equiatomic concentration in the studied thickness regime of up to 15 ML. In order to address the magnetic order in epitaxial NiMn films, MOKE measurements were extended to NiMn/Co bilayers. If AFM order is established in the NiMn layer, these bilayers ought to show the well-known characteristic of coercivity enhancement resulting from the interfacial exchange interaction between the AFM and the FM layer. This indirect evidence of AFM order in equiatomic NiMn films was indeed provided for certain values of $x$ by our MOKE experiments on $Ni_xMn_{100-x}$/6 ML Co/Cu(001). The hysteresis loops were measured in longitudinal geometry at 300 K with the external magnetic field $H$ applied along the [100] direction. Though this is the magnetic hard axis of Co on Cu(001),[30] previous experiments using the same setup showed no difference of the remanence for measurements with $H$ applied along the ⟨100⟩ hard and ⟨110⟩ easy axes.[31] The $Ni_xMn_{100-x}$ films were deposited on magnetically saturated 6 ML Co/Cu(001). The thickness of the $Ni_xMn_{100-x}$ films was increased by a subsequent deposition after each MOKE measurement in order to trace the thickness dependence of the coercivity $H_c$. The results of various thickness series are compiled in Fig. 7. The noncovered 6 ML Co/Cu(001) samples exhibited square-shaped hysteresis loops [cf. Fig. 8(b)] with an $H_c$ of about 0.4 kA/m. The shape and width of the hysteresis loop of the bilayer system remained unchanged upon covering the 6 ML Co film with a $Ni_{65}Mn_{35}$ film (open symbols), independent of its thickness up to the maximum studied thickness of 21 ML. A different behavior was observed in the case of equiatomic and nearly equiatomic NiMn films, as can be seen by the filled symbols. A distinct broadening of the hysteresis loops, which further increases with the coverage $t_{NiMn}$, was found above $t_{NiMn}$=8 ML. As an example, the inset compares the nonexpanded hysteresis loop (i) of 10 ML $Ni_{65}Mn_{35}$/6 ML Co/Cu(001) with the broadened hysteresis loop (ii) of 10 ML $Ni_{50}Mn_{50}$/6 ML Co/Cu(001).

A similar manifestation of the interfacial exchange interaction in epitaxial bilayers of equiatomic NiMn and Co was observed for the reversed deposition sequence, i.e., for Co on NiMn/Cu(001). The previous experiment has shown that the

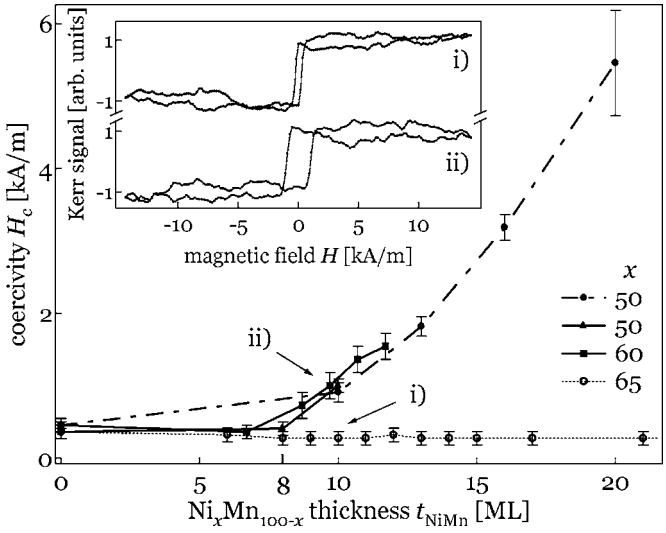


FIG. 7. Coercivity vs $Ni_xMn_{100-x}$ thickness obtained from a thickness series of $Ni_xMn_{100-x}$ on 6 ML Co/Cu(001) for $x=50$ (two separate series), 60, and 65. The inset shows the hysteresis loops of a bilayer composed of a nonequiatomic 10 ML $Ni_{65}Mn_{35}$ film (i) and of a 10 ML $Ni_{50}Mn_{50}$ film (ii). Note the onset of coercivity enhancement for equiatomic NiMn films at 8 ML.

magnetization reversal of the Co film is unchanged in comparison to Co/Cu(001) if the Co film is in contact with a thick $Ni_{65}Mn_{35}$ film. This property seems to be independent of the actual deposition sequence, as can be deduced from Fig. 8, showing the hysteresis loops at 300 K of 6 ML Co/13.2 ML $Ni_{65}Mn_{35}$/Cu(001) in comparison to the one of 6 ML Co/Cu(001). As can be seen, both MOKE loops are similar in shape. Note also the lower noise level in comparison to Fig. 7 resulting from the fact that now the Co film plays the role of the top layer. This gives rise to a larger signal-to-noise ratio of the magneto-optical response. In full agreement with the results of equiatomic NiMn films on Co/Cu(001), coercivity enhancement was found at 300 K for Co deposited on sufficiently thick equiatomic NiMn/Cu(001). As before, the top layer was subsequently increased in thickness after each MOKE measurement. Figure 9(a) shows three selected hysteresis loops of Co/12.2 ML NiMn/Cu(001) for Co layer thicknesses $t_{Co}$ of 7, 14, and 21

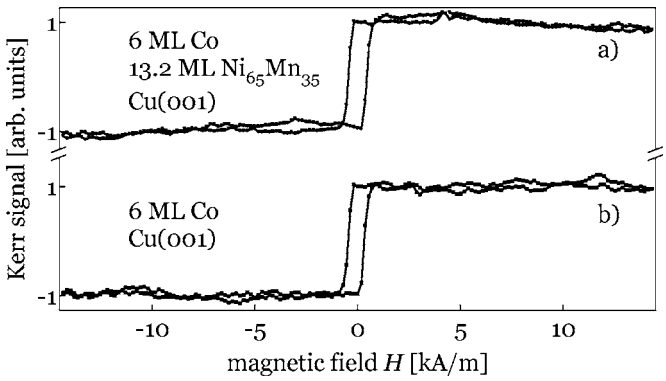


FIG. 8. Square-shaped hysteresis loops of (a) 6 ML Co/13.2 ML $Ni_{65}Mn_{35}$/Cu(001) and (b) 6 ML Co/Cu(001).

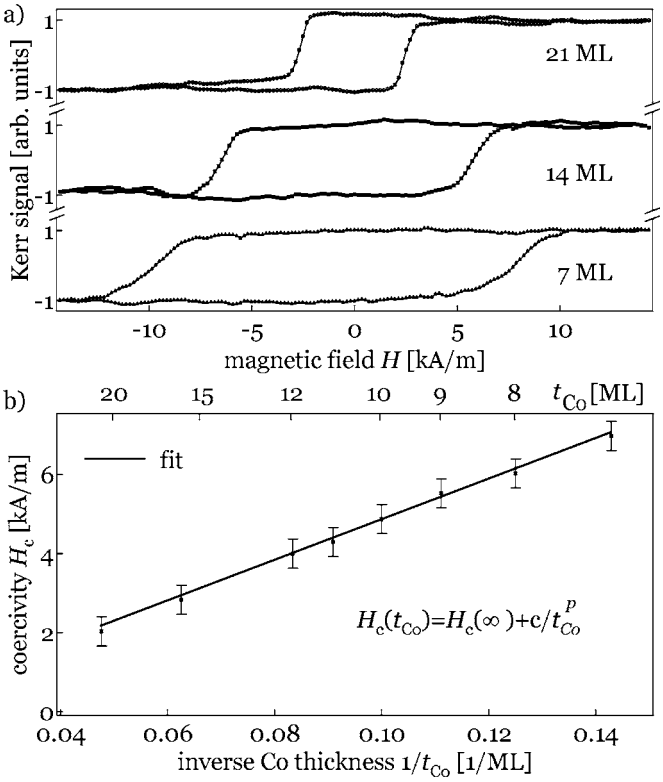


FIG. 9. Hysteresis loops (a) of Co/12.2 ML NiMn/Cu(001) for Co layer thicknesses $t_{Co}$ of 7, 14, and 21 ML. Coercivity (b) of this bilayer system vs $1/t_{Co}$. The power-law fit yielded an exponent of $p=1.05\pm0.25$.

ML. The choice of $t_{NiMn}=12.2$ ML was made since AFM order in equiatomic NiMn is expected from Fig. 7 at 300 K for $t_{NiMn}>8$ ML. As mentioned above, no Kerr signal was measured for $t_{Co}=0$. The strong coercivity enhancement of our Co/NiMn/Cu(001) system in comparison to the reference hysteresis loop of 6 ML Co/Cu(001) in Fig. 8(b) is obvious. One notices a decreasing $H_c$ with increasing $t_{Co}$. The results of the coercivity analysis of the complete thickness series is shown by an $H_c$ vs $1/t_{Co}$ plot in Fig. 9(b). A $1/t_{Co}$ dependence of $H_c$ can already be deduced from the constant slope in this plot. However, the data were fitted with the general power-law function $H_c(t_{Co})=H_c(\infty)+c/t_{Co}^p$, where $H_c(\infty)$ and $c$ denote the coercivity for infinite Co layer thickness and a constant factor, respectively. The fitting yielded an exponent of $p=1.05\pm0.25$.

As mentioned above, Fig. 9(a) depicts the loops of as-grown Co/NiMn bilayers, which were not field cooled, thus no exchange bias was set. However, the hysteresis loops exhibit a slight shift towards negative fields. This accidental exchange bias is most pronounced in the case of the thinnest Co layer of 7 ML, and its dependence on the thickness of the FM layer is similar to that of the coercivity. So far, we have not studied the origin of this effect in detail. It may be induced by a small nonzero magnetic field during the deposition, or by slight temperature variations during the course of the measurements, which may set exchange bias if the blocking temperature of the bilayer is close to the measuring temperature (300 K). It could also stem from a training effect

due to previous Kerr measurements since the sample remains in positive remanence after the measurement of each loop.

## IV. DISCUSSION

Our MEED study of $Ni_xMn_{100-x}$ on Cu(001) revealed a layer-by-layer growth mode at 300 K for a wide concentration range. In fact the MEED oscillations for the growth of alloys with $x>40$ decay much slower with coverage than in the case of the growth of pure Ni on Cu(001), which is characterized by a dominant multilayer growth at coverages above 6 ML.[32] Our observation of an improved layer-by-layer growth is consistent with the growth study of Ni-rich $Ni_xMn_{100-x}$ films ($x \geqslant 83$) on Cu(001) by Thamankar *et al.*,[23] who found oscillations of the reflective high-energy electron diffraction intensity for coverages up to 17 ML. As the Mn content increases, the growth mode smoothly changes to the well-known non-layer-by-layer growth mode of Mn on Cu(001).[33] A closer inspection of Fig. 1 reveals the presence of an additional oscillation with a period of two monolayers in the MEED curves from alloys with Ni concentrations not too far away from the equiatomic concentration. The two-layer periodicity is best seen in the curve with $x=45$. However, this additional periodicity has not yet been studied in detail, and remains to be investigated by the combination with a more dedicated technique such as scanning tunneling microscopy.

As found by LEED, equiatomic NiMn films grown at 300 K on Cu(001) are characterized by a $c(2\times2)$ superstructure. This superstructure can be explained by a bulklike crystal structure which can be stabilized due to the small lattice mismatch ($a_{NiMn}/a_{Cu}-1$) of the $L1_0$ bulk phase with respect to the Cu(001) substrate with a lattice constant of 3.61 Å. The lattice mismatch of the bulk $c$ axis and the two $a$ axes is −2.5% and +3.6%, respectively. A bulklike crystal structure is compatible with an out-of-plane or an in-plane orientation of the bulk $c$ axis in NiMn on Cu(001). The first case would need a demixing of Ni and Mn atoms during growth, leading to alternating planes of Ni and Mn along the growth direction, and a uniform compressive strain of both bulk $a$ axes. Such a film structure would give rise to a $p(1\times1)$ LEED pattern, which is in contradiction to our findings. In addition, the $c$ axis, which in bulk is the shortest, would be the largest axis in this structure as a result of the lateral compression of both $a$ axes under the assumption of equal atomic volumes in bulk and film. This leaves the second case, which is indeed consistent with our LEED $I(E)$ results. Here, the (001) planes consist of an equal amount of Ni and Mn atoms, arranged in a chessboard structure, similar to the $c(2\times2)$ surface alloys of CuPd,[34] CuMn,[25] CuAu (Ref. 35) on Cu(001), and NiMn (Ref. 20) on Ni(001). Figure 10 illustrates the film's bulklike crystal structure with the bulk $c$ axis lying along the [100] direction. As can be seen, the substrate imposes a nonuniform lattice strain. In the film plane, the $c$ axis and one of the $a$ axes experience a tensile and compressive strain, respectively. The lattice constant along the surface normal is twice the interlayer spacing, i.e., 3.74 Å, as determined from our LEED $I(E)$ analysis. This distance coincides very well with the bulk value of the $a$ axis. Using this value and the strained

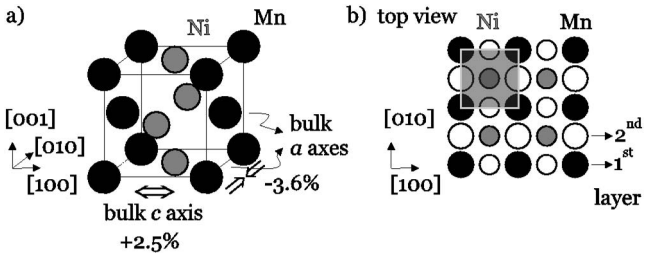


FIG. 10. Bulklike structure model of chemically ordered $c(2\times2)$ NiMn on Cu(001): Ni and Mn atoms are shown by gray and larger black spheres, respectively. The bulk $c$ axis lies in the surface plane and experiences a lateral expansion in order to accommodate the lattice mismatch with the substrate (a). The sketch in (b) shows a top view of the atoms in the first (filled symbols) and second (open symbols) layer. The $c(2\times2)$ surface unit cell is indicated by a square. Note the twofold symmetry of the in-plane film structure.

in-plane lattice constant, i.e., the lattice constant of Cu(001), yields an average atomic volume of the film unit cell of equiatomic $c(2\times2)$ NiMn/Cu(001) of 48.7 Å,[3] which is nearly the same as the bulk value of 49.2 Å.[3] This indicates an isochoric distortion of the bulk unit cell.

We may also comment on the dependence of the film's vertical lattice spacing on the composition. The interlayer spacing was found to be constant for Mn-rich films, and to decrease with $x$ above $x\sim30$ (cf. Fig. 4). This agrees qualitatively with the lattice constant of bulk $Ni_xMn_{100-x}$, which monotonically decays with $x$ from 3.70 Å at $x=19$ to 3.53 Å at $x=94$, in addition to a change of slope at $x\sim40$.[36]

The proposed structure model of $c(2\times2)$ NiMn/Cu(001) with a bulklike crystal structure throughout the whole film thickness is characterized by a twofold in-plane symmetry and an $AB$ stacking sequence along the growth direction, as can be seen from the projection of the topmost two layers onto the surface plane in Fig. 10(b). However, our LEED study revealed a fourfold superstructure pattern, independent of thickness in the range from 1 to 15 ML and more (cf. Fig. 2). This indicates an equal distribution of two structural 90° domains, which are characterized by a mutually orthogonal in-plane orientation of the bulk $c$ axis, on the fourfold symmetric Cu(001) substrate. These domains have a lateral dimension of about 5 nm, as observed by a recent spin-polarized scanning tunneling microscopy study.[37]

Our structure model is similar to the structure model of 1–8 ML $c(2\times2)$ NiMn/Ni(001),[20] which is characterized by a different but also nonuniform lattice strain. This system is known for its large outward relaxations of the Mn atoms of 0.25 Å in the topmost NiMn layer.[21] Thus, it is reasonable to expect a similar behavior for our system. In fact, a preliminary dynamical analysis of a large set of LEED $I(E)$ curves of 12 and 15 ML $c(2\times2)$ NiMn/Cu(001) supports our structural model and suggests indeed an outward relaxation of the topmost Mn atoms.[38]

One may argue that a chemically ordered surface layer on top of a chemically disordered film does also lead to a $c(2\times2)$ pattern due to the surface sensitivity of LEED. This is an unreasonable film structure since the growth of such a film would have to be accompanied by an order-disorder

transition of the layer covered by the growing $c(2\times2)$ layer. Experimental indications of the presence of chemical order throughout the whole film thickness were obtained by exposing a 7 ML $c(2\times2)$ NiMn film on Cu(001) at 300 K to CO gas at a partial pressure of $5\times10^{-6}$ mbar for 3 min. No change of the relative superstructure spot intensities in comparison to the integer spot intensities was observed. Repeating the CO exposure procedure for an additional 11 minutes led to the same result. If the superstructure spots had disappeared, they would have stemmed from the ordering of the topmost layer only.

An additional argument in favor of an ordered film structure is based on the thermodynamical properties of bulk NiMn. The equiatomic bulk alloy system has a tendency towards ordering.[39] It is reasonable to assume a similar behavior of the film phase, which has indeed been shown for the case of thin NiMn films on Ni(001).[20]

A $c(2\times2)$ magnetic order can probably be excluded as the origin of the half-order LEED spots because of their relatively large intensity in comparison to the integer order spots. Such a magnetic order would give rise to $c(2\times2)$ spot intensities of the order of a few hundredths of the integer order spot intensity only, as shown experimentally for AFM NiO(100) (Ref. 40) and theoretically for 1 ML AFM Cr/Pd(001).[41]

The interpretation of $c(2\times2)$ spots as a result of the chemical order in NiMn films on Cu(001) in combination with a relaxation in the topmost layer is in full agreement with the bulk phase diagram of $Ni_xMn_{100-x}$,[13] exhibiting an $L1_0$ phase at the equiatomic concentration. In addition, the $p(1\times1)$ LEED patterns of Ni- and Mn-rich films on Cu(001) suggest a chemically disordered structure, i.e., a random distribution of Ni and Mn atoms on the lattice, which is also predicted by the bulk-phase properties.

We also observed a weak but noticeable $c(2\times2)$ LEED pattern from equiatomic NiMn deposited on a Co/Cu(001) sample (cf. Fig. 6). This indicates a certain degree of structural similarity, if not even equality, with $c(2\times2)$ NiMn films on Cu(001). This behavior is not surprising since a Co film in the monolayer thickness regime adopts the Cu(001) in-plane lattice constant.[29,42] However, we cannot prove this due to the lack of a detailed structural analysis by dynamic LEED $I(E)$.

As already mentioned, the bulk $L1_0$ phase of NiMn is characterized by an AFM spin structure with a Néel temperature far above room temperature. The hysteresis loops obtained from bilayers of FM Co and equiatomic NiMn revealed the fingerprints of AFM order in the alloy, namely coercivity enhancement, which results from the exchange interaction at the interface.[2,3,43,44] The thickness study of equiatomic NiMn on 6 ML Co/Cu(001) suggests that the AFM order is established at 300 K above a critical film thickness of about 8 ML. The NiMn film is believed to be paramagnetic (PM) below this critical thickness, similar to single-crystalline FeMn films,[5] as concluded from the similar shapes of the hysteresis loops of thin NiMn films in contact with a Co film and a single Co film on Cu(001). No significant change of the hysteresis loop width has also been observed for bilayers that contain a Ni-rich alloy film with $x=65$. This is a strong indication for the absence of a magnetic order in the alloy, which has to be attributed to the chemical disorder, as concluded from the low intensity of the superstructure LEED spots. This correlation between chemical and magnetic order in the alloy film is in agreement with the properties of the bulk phase,[13,15,19] since Ni-rich bulk alloys with $x=65$ are characterized by a predominant disordered fcc structure with no magnetic order. A small amount of the $L1_0$ phase is also present in bulk samples of this composition. However, it disappears completely for higher $x$.[13] The Néel temperature of the film and therefore the critical thickness of AFM ordering is probably relatively insensitive to $x$, since $T_N$ of the bulk does only slightly decrease from 1070 K by less than 60 K upon changing the Ni content within the narrow $L1_0$ phase from $x=50$ in either direction by 5 at. %.[14] This is in contrast to $Fe_xMn_{100-x}$ films, where $T_N$ was found to significantly fall off with Fe content within the range studied from 45 to 65 at. % Fe.[5]

The coercivity of our Co/NiMn/Cu(001) system decreases with the Co thickness $t_{Co}$. This behavior is generally attributed to the interfacial nature of the magnetic interaction. Our analysis yields a $1/t_{Co}^{p}$ dependence with an exponent $p$ close to one, which proves the magnetic interaction with the NiMn film as the source of the coercivity enhancement. A similar behavior was found for single-crystalline Co/AFM FeMn/Cu(001) systems.[5] One might be tempted to use the model describing coercivity of AFM/FM systems by Stiles *et al.*[45] for the explanation of this thickness dependence. According to their model, an exponent of one stems from energy losses due to irreversible processes in the AFM layer during the reversal of the magnetization. This is the dominant contribution at nonzero temperatures besides the second effect of an inhomogeneous reversal in the FM layer, which gives rise to an exponent of two at low temperatures. However, their model describes the magnetization reversal of a polycrystalline bilayer, in which the easy axes of the AFM domains are randomly distributed in space. This is obviously not a correct description of our single-crystalline bilayer system, although there may indeed exist two easy axes in the AFM NiMn layer as a result of two structural 90° domains, if a bulklike AFM spin structure with an in-plane orientation of the spins normal to the bulk $c$ axis is considered.[14–16,18] Such a bulklike AFM spin structure gives rise to uncompensated (001) planes in which the moments point along one of the four $\langle100\rangle$ in-plane directions. This is similar to the PtMn/Fe system, where the chemically ordered $L1_0$ PtMn film is characterized by the presence of AFM domains with a compensated interface spin structure resulting from structural domains with an orthogonal in-plane orientation of their $c$ axes.[46] Finally, we want to emphasize that the presence of these structural domains in the AFM layer may have an effect on the mechanism of exchange bias, as found for $MnF_2$/Fe (Refs. 47 and 48) and $FeF_2$/Fe.[47]

## V. SUMMARY

In this work we have studied the growth, structure, and magnetic properties of $Ni_xMn_{100-x}$ films, with emphasis on equiatomic alloys due to their potential use as an AFM layer

in AFM/FM model systems for the investigation of phenomena related to exchange bias. Smooth single-crystalline NiMn films with a high structural perfection can be stabilized on Cu(001) at 300 K. The pronounced layer-by-layer growth of NiMn on Cu(001) is an advantage because it allows us to tune the interface morphology of Co/NiMn bilayers on Cu(001). The $c(2\times2)$ LEED patterns, found for equiatomic NiMn films on Cu(001), can be explained by a bulklike $L1_0$ film structure. The film is characterized by a nonuniform strain due to the in-plane orientation of the bulk $c$ axis. The $p(1\times1)$ LEED patterns of nonequiatomic films suggest the absence of chemical order in these films, which is in agreement with the bulk-phase properties. Weaker $c(2\times2)$ LEED patterns were observed for NiMn deposited on Co/Cu(001), probably resulting from the rougher surface and not from a lower chemical order, as concluded from the absence of MEED oscillations.

The magnetic characterization was performed by means of MOKE. Our thickness study suggests that AFM order is established in equiatomic NiMn films at 300 K above a critical thickness of about 8–10 ML, as concluded from the coercivity enhancement of NiMn/Co bilayers on Cu(001). The study of Co/NiMn on Cu(001) revealed that the coercivity scales inversely with the Co thickness.

## ACKNOWLEDGMENTS

We wish to thank C. L. Gao, C. Tusche, A. Winkelmann, and W. Wulfhekel for stimulating discussions, and F. Helbig for technical assistance.

*Present address: Freie Universität Berlin, Institut für Experimentalphysik, Arnimallee 14, D-14195 Berlin, Germany.
†Present address: Clarendon Laboratory, Department of Physics, University of Oxford, Parks Road, Oxford, OX1 3PU, UK.

[1] W. H. Meiklejohn and C. P. Bean, Phys. Rev. **102**, 1413 (1956).
[2] J. Nogués and I. K. Schuller, J. Magn. Magn. Mater. **192**, 203 (1999).
[3] A. E. Berkowitz and K. Takano, J. Magn. Magn. Mater. **200**, 552 (1999).
[4] S. S. P. Parkin, K. P. Roche, M. G. Samant, P. M. Rice, R. B. Beyers, R. E. Scheuerlein, E. J. O'Sullivan, S. L. Brown, J. Bucchigano, D. W. Abraham, Yu Lu, M. Rooks, P. L. Trouilloud, R. A. Wanner, and W. J. Gallagher, J. Appl. Phys. **85**, 5828 (1999).
[5] F. Offi, W. Kuch, and J. Kirschner, Phys. Rev. B **66**, 064419 (2002).
[6] W. Kuch, L. I. Chelaru, F. Offi, J. Wang, M. Kotsugi, and J. Kirschner, Phys. Rev. Lett. **92**, 017201 (2004).
[7] S. Mao, N. Amin, and E. Murdock, J. Appl. Phys. **83**, 6807 (1998).
[8] J. P. Nozières, S. Jaren, Y. B. Zhang, A. Zeltser, K. Pentek, and V. S. Speriosu, J. Appl. Phys. **87**, 3920 (2000).
[9] M. F. Toney, M. G. Samant, T. Lin, and D. Mauri, Appl. Phys. Lett. **81**, 4565 (2002).
[10] T. Lin, D. Mauri, N. Staud, C. Hwang, J. K. Howard, and G. L. Gorman, Appl. Phys. Lett. **65**, 1183 (1994).
[11] S. Groudeva-Zotova, D. Elefant, R. Kaltofen, J. Thomas, and C. M. Schneider, J. Magn. Magn. Mater. **278**, 379 (2004).
[12] F. J. Espinosa-Faller, R. C. Howell, A. J. Garcia-Adeva, S. D. Conradson, A. Y. Ignatov, T. A. Tyson, R. F. C. Farrow, and M. F. Toney, J. Phys. Chem. B **109**, 10406 (2005).
[13] L. Ding, P. F. Ladwig, X. Yan, and Y. A. Chang, Appl. Phys. Lett. **80**, 1186 (2002).
[14] L. Pál, E. Krén, G. Kádár, P. Szabó, and T. Tarnóczi, J. Appl. Phys. **39**, 538 (1968).
[15] J. S. Kasper and J. S. Kouvel, J. Phys. Chem. Solids **11**, 231 (1959).
[16] D. Spišák and J. Hafner, J. Phys.: Condens. Matter **11**, 6359 (1999).
[17] V. V. Godlevsky and K. M. Rabe, Phys. Rev. B **63**, 134407 (2001).
[18] A. Sakuma, J. Magn. Magn. Mater. **187**, 105 (1998).
[19] E. Krén, E. Nagy, I. Nagy, L. Pál, and P. Szabó, J. Phys. Chem. Solids **29**, 101 (1968).
[20] M. Wuttig, T. Flores, and C. C. Knight, Phys. Rev. B **48**, 12082 (1993).
[21] M. Wuttig, C. C. Knight, T. Flores, and Y. Gauthier, Surf. Sci. **292**, 189 (1993).
[22] W. L. O'Brien and B. P. Tonner, Phys. Rev. B **51**, 617 (1995).
[23] R. Thamankar, S. Bhagwat, and F. O. Schumann, J. Phys.: Condens. Matter **16**, 6029 (2004).
[24] F. Baudelet, M.-T. Lin, W. Kuch, K. Meinel, B. Choi, C. M. Schneider, and J. Kirschner, Phys. Rev. B **51**, 12563 (1995).
[25] M. Wuttig, Y. Gauthier, and S. Blügel, Phys. Rev. Lett. **70**, 3619 (1993).
[26] S. Tanuma and C. J. Powell, Surf. Interface Anal. **17**, 911 (1991).
[27] W. Platow, U. Bovensiepen, P. Poulopoulos, M. Farle, K. Baberschke, L. Hammer, S. Walter, S. Müller, and K. Heinz, Phys. Rev. B **59**, 12641 (1999).
[28] C. M. Schneider, A. K. Schmid, P. Schuster, H. P. Oepen, and J. Kirschner, *Magnetism and Structure in Systems of Reduced Dimension* (Plenum Press, New York, 1993).
[29] J. R. Cerdá, P. L. de Andres, A. Cebollada, R. Miranda, E. Navas, P. Schuster, C. M. Schneider, and J. Kirschner, J. Phys.: Condens. Matter **5**, 2055 (1993).
[30] C. M. Schneider, P. Bressler, P. Schuster, J. Kirschner, J. J. de Miguel, R. Miranda, and S. Ferrer, Vacuum **41**, 503 (1990).
[31] X. Gao, M. Salvietti, W. Kuch, C. M. Schneider, and J. Kirschner, J. Electron Spectrosc. Relat. Phenom. **113**, 137 (2001).
[32] J. Shen, J. Giergiel, and J. Kirschner, Phys. Rev. B **52**, 8454 (1995).
[33] T. Flores, M. Hansen, and M. Wuttig, Surf. Sci. **279**, 251 (1992).
[34] S. C. Wu, S. H. Lu, Z. Q. Wang, C. K. C. Lok, J. Quinn, Y. S. Li, D. Tian, F. Jona, and P. M. Marcus, Phys. Rev. B **38**, 5363 (1988).
[35] Z. Q. Wang, Y. S. Li, C. K. C. Lok, J. Quinn, F. Jona, and P. M. Marcus, Solid State Commun. **62**, 181 (1987).
[36] W. B. Pearson, *A Handbook of Lattice Spacings and Structures of Metals and Alloys* (Pergamon Press, Oxford, 1964).
[37] C. L. Gao (unpublished).

[38] A. Winkelmann (private communication).
[39] M. Wuttig and X. Liu, *Ultrathin Metal Films—Magnetic and Structural Properties* (Springer, Berlin, 2004), p. 319.
[40] W. Palmberg, R. E. DeWames, and L. A. Vredevoe, Phys. Rev. Lett. **21**, 682 (1968).
[41] E. Tamura, S. Blügel, and R. Feder, Solid State Commun. **65**, 1255 (1988).
[42] E. Navas, P. Schuster, C. M. Schneider, J. Kirschner, A. Ceballada, C. Ocal, R. Miranda, J. Cerdá, and P. de Andrés, J. Magn. Magn. Mater. **121**, 65 (1993).
[43] R. L. Stamps, J. Phys. D **33**, R247 (2000).
[44] M. Kiwi, J. Magn. Magn. Mater. **234**, 584 (2001).
[45] M. D. Stiles and R. D. McMichael, Phys. Rev. B **63**, 064405 (2001).
[46] A. Mougin, J. Borme, R. L. Stamps, A. Marty, P. Bayle-Guillemaud, Y. Samson, and J. Ferré, Phys. Rev. B **73**, 024401 (2006).
[47] M. R. Fitzsimmons, P. Yashar, C. Leighton, I. K. Schuller, J. Nogués, C. F. Majkrzak, and J. A. Dura, Phys. Rev. Lett. **84**, 3986 (2000).
[48] M. J. Pechan, D. Bennett, N. Teng, C. Leighton, J. Nogués, and I. K. Schuller, Phys. Rev. B **65**, 064410 (2002).